American Mineralogist, Volume 65, pages 285–301, 1980

Subsolidus and liquidus phase relationships in the system CaO–SiO_2–CO_2 to 30 kbar with geological applications

WUU-LIANG HUANG[1]

Department of Geology, National Taiwan University
Taipei, Taiwan, Republic of China

PETER J. WYLLIE

Department of Geophysical Sciences, University of Chicago
Chicago, Illinois 60637

AND C. E. NEHRU

Department of Geology
Brooklyn College of the City University of New York
Brooklyn, New York 11210

Abstract

Mixtures of crystalline $CaCO_3$, Ca_2SiO_4, $CaSiO_3$, quartz, and spurrite were reacted between 7 and 27 kbar. The results, combined with other published data, provide a *PT* projection for the system CaO–SiO_2–CO_2 from 1 bar to 30 kbar, and a series of isobaric liquidus diagrams giving the changes in composition of eutectic and peritectic liquids in the univariant reactions as a function of pressure. The assemblage calcite + quartz dissociates producing wollastonite + CO_2 at pressures below an invariant point at 18.5 kbar, 1,325°C; at this point, the univariant dissociation reaction meets the fusion curve for wollastonite + CO_2 = quartz + liquid; at higher pressures, calcite + quartz melts incongruently to liquid + CO_2, and there is in addition a eutectic reaction between calcite, wollastonite, and quartz. The thermal barrier on the liquidus associated with the congruent melting of larnite in the system CaO–SiO_2 is eliminated by solution of a few percent CO_2 at pressures greater than about 1 kbar; the CO_2 causes expansion of the liquidus fields for calcite and wollastonite until they meet and exclude both spurrite and larnite from the CO_2-saturated liquidus field boundary. The liquidus diagrams show limiting conditions for coprecipitation of calcite and wollastonite in carbonatite magmas. Liquids produced by partial melting of siliceous limestones (±wollastonite) at pressures above about 15 kbar have compositions near 50% $CaCO_3$, 50% $CaSiO_3$. There is a good prospect that some subducted pelagic limestone might escape dissociation and melting and be carried to considerable depths for long-term storage of carbon in the mantle either as aragonite (reacting to dolomite or magnesite), or as diamond if the carbonate is reduced.

Introduction

Carbon dioxide is a component of interest to geophysicists concerned with the mantle, as well as to geologists concerned with the deposition of limestones and petrologists concerned with the metamorphism of limestones and the origin and evolution of kimberlites and carbonatites. Evidence that CO_2 is transported from the mantle by magmas and rocks was reviewed by Wyllie (1977) and Eggler (1978), and results reported by Green and Radcliffe (1975) and Delaney *et al.* (1978) suggest that CO_2 may predominate over H_2O in some environments.

Speculation about the possible effects of CO_2 on magma generation and other mantle processes has been accompanied by experimental efforts to evaluate its influence (for reviews see Boettcher, 1975; Wyllie, 1977; Eggler, 1978). Wyllie (1977) summa-

[1] Present address: Lunar and Planetary Institute, 3303 NASA Road 1, Houston, Texas 77058.

0003–004X/80/0304–0285$02.00

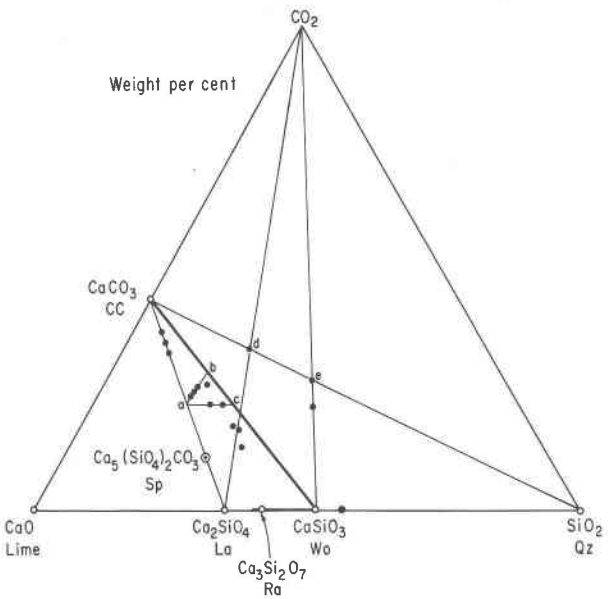

Fig. 1. Starting mixtures and composition joins used in the system $CaO–SiO_2–CO_2$.

rized various experimental approaches to the problem, including the study of peridotites and possible primary magmas with CO_2 and other volatile components, the study of synthetic peridotite mineral assemblages with CO_2, the study of carbonate melting and dissociation reactions, and the study of silicate–carbonate systems that include minerals related to the natural mantle minerals.

The system $CaO–MgO–SiO_2–CO_2$, which includes forsterite, enstatite, and diopside, is the simplest system that can be used as a basis for interpretation of relationships between mantle peridotite, kimberlite, and carbonatite. Wyllie and Huang (1975, 1976a) presented comprehensive, partly schematic phase relationships for this system, which provide a framework for the location of needed experimental studies, and for petrological interpretations and applications. These papers were based on our published data on carbonate–silicate systems, much unpublished data from the composition join $MgSiO_3–CaSiO_3–MgCO_3–CaCO_3$ (see Huang and Wyllie, 1974a), data from Eggler (1974, 1975) on silicate–CO_2 reactions, and our results for the system $CaO–SiO_2–CO_2$ presented in detail in this paper. Eggler (1976, 1978) presented results of a detailed study of the effect of CO_2 on parts of the composition join $Mg_2SiO_4–MgSiO_3–CaMgSi_2O_6–Ca_2SiO_4–CaMgO_2–CO_2$ in the system $CaO–MgO–SiO_2–CO_2$.

The system $CaO–SiO_2–CO_2$ forms one side of the quaternary tetrahedron for the model mantle system $CaO–MgO–SiO_2–CO_2$. It serves as a model for the phase relationships in more complex silicate–CO_2 systems, where subsolidus carbonation reactions intersect the solidus for silicate–CO_2 melting reactions and introduce primary carbonate minerals alongside silicate minerals on the liquidus at higher pressures. The system also has direct bearing on the fate of pelagic limestones that may be subducted beneath ocean trenches, and on the crystallization of carbonatite magmas.

Experimental methods

The starting materials were: (1) $CaCO_3$, "Specpure" calcite from Johnson, Matthey Co., previously dried at 600°C; (2) synthetic $CaSiO_3$ and $CaSiO_4$, crystallized hydrothermally from gels, previously dried at 1,000°C; (3) SiO_2, purified Lisbon quartz; (4) natural spurrite, Tres Hermanas District, New Mexico. Starting mixtures of these fine-grained materials with the compositions given in Figure 1 were ground under acetone. The mixtures were loaded into platinum capsules and dried at 500°C for 2 hours, immediately prior to sealing.

Experiments were performed in 0.5″ diameter piston–cylinder apparatus, with pyrex furnace assemblies to maintain a dry environment, and piston-out method (Irving and Wyllie, 1975). For our first results in this system (Huang and Wyllie, 1974a, 1975a) we assumed that no friction correction was required, following Boyd *et al.* (1967), but we determined subsequently that with pyrex sleeve in the assembly, nominal pressures required a correction for anvil effects of −3 kbar (Huang and Wyllie, 1975b). The results tabulated and plotted at 7 and 27 kbar had been planned for 10 and 30 kbar, respectively. The corrected pressures are considered accurate to ±5%. Temperatures are precise to ±5°C and accurate to better than ±15°C.

The quenched charges were examined with binocular microscope for physical evidence of the former presence of liquid or vapor phase, then crushed fragments in immersion oil were studied with a petrographic microscope. X-ray diffraction patterns were obtained for the powdered samples.

The phases identified in the run products are: calcite (CC), well-crystallized rhombs in subsolidus runs, larger and commonly rounded in the presence of liquid; larnite (La), euhedral grains with very high relief; γ-Ca_2SiO_4, of lower relief, is produced by inversion of larnite during the quench (see also Wyllie and Haas, 1965; Boettcher and Wyllie, 1969; the mechanism of the inversion, producing apparently

Table 1. Experimental results for the join Ca_2SiO_4–$CaSiO_3$

Run	Starting Composition wt % Ca_2SiO_4	$CaSiO_3$	Press. Kb	Temp. °C	Time min.	Results Assemblage at P and T
251	35	65	7	1400	80	La + Pwo
262	35	65	7	1425	18	La + Pwo
260	10	90	7	1450	20	La + Pwo + L
253	15	85	7	1450	20	La + Pwo
261	35	65	7	1450	20	La + Pwo + L
256	10	90	7	1500	15	Pwo + L
254	15	85	7	1500	15	Pwo + L
257	25	75	7	1500	15	Pwo + L
259	35	65	7	1500	15	L
258	45	55	7	1500	15	La + L
255	15	85	7	1500	9	L
263	45	55	7	1600	8	La + L
264	45	55	7	1650	5	L
776	15	85	27	1450	30	La + Wo-II
815	30	70	27	1450	30	La + Wo-II
783	7.5	92.5	27	1500	20	La + Wo-II
777	15	85	27	1500	20	La + Wo-II
781	15	85	27	1550	20	La + Wo-II
839	30	70	27	1550	15	La + Wo-II
784	7.5	92.5	27	1600	10	La + Wo-II + L
840	30	70	27	1600	10	La + Wo-II + L
788	7.5	92.5	27	1650	5	L
796	15	85	27	1650	5	L
798	30	70	27	1650	5	La + L
791	50	50	27	1650	10	La + L
802	30	70	27	1700	5	La + L
814	70	30	27	1700	3	La + L

Table 2. Experimental results for the join $CaSiO_3$–SiO_2

Run	Starting Composition wt % $CaSiO_3$	SiO_2	Press. Kb	Temp. °C	Time min.	Results Assemblage at P and T
1041	90	10	27	1475	40	Wo-II + Qz
1042	90	10	27	1500	30	Wo-II + Qz
1040	90	10	27	1525	30	Wo-II + L
1037	90	10	27	1575	20	Wo-II + L

random proportions of γ-Ca_2SiO_4, is not clear to us); polymorphs of $CaSiO_3$, wollastonite-I (Wo-I), wollastonite-II (Wo-II), and parawollastonite (P_{wo}) with properties described by Huang and Wyllie (1975a); quartz (Qz), easily identified by its low refractive index and X-ray diffraction pattern; quenched liquid (L), identified by textures described in similar systems (Wyllie and Tuttle, 1960; Wyllie and Haas, 1965); vapor (V), identified by the emission of gas when capsules from subsolidus runs were punctured, and by small hemispherical depressions on the surface of a charge quenched from above the solidus—these represented vapor bubbles in liquid; spurrite (Sp) starting material broke down during runs.

Experimental results

The results of experimental runs are listed in Tables 1 through 6, and plotted in Figures 2 through 4, with the composition joins through the ternary system corresponding to those drawn in Figure 1.

The system Ca_2SiO_4–SiO_2 (Tables 1 and 2, Fig. 2)

The results at 1 bar in Figure 2A are taken from the system CaO–SiO_2 as drawn by Wyllie and Haas (1965). Rankinite (Ra), tridymite (Tr), and cristobal-

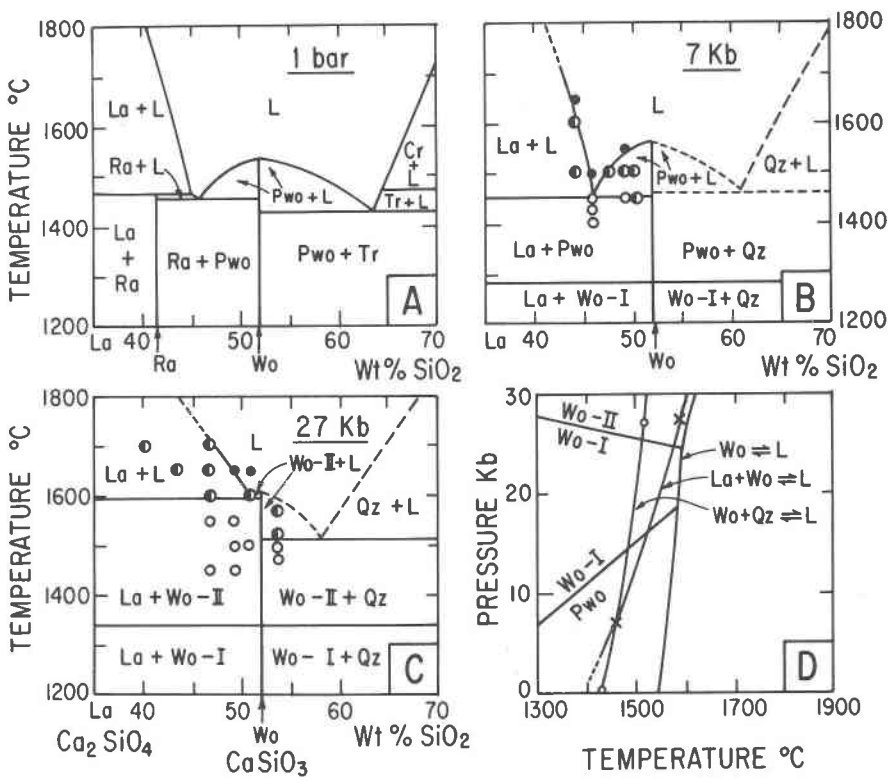

Fig. 2. Experimental results for parts of CaO–SiO_2.

Table 3. Experimental results for the join $CaCO_3$–$CaSiO_3$

Run	Starting Composition wt % $CaCO_3$	$CaSiO_3$	Corrected Press. Kb	Temp. °C	Time min.	Results Assemblages at P and T
208	50	50	7	1150	120	CC + Wo-I
201	55.9	44.1*	7	1200	65	CC + Wo-I
218	65	35	7	1200	60	CC + Wo-I
206	75	25	7	1200	55	CC + Wo-I
219	65	35	7	1225	40	CC + L
202	50	50	7	1250	45	Wo-I + L
210	55.9	44.1	7	1250	45	Wo-I + L
221	65	35	7	1250	35	L
213	75	25	7	1250	45	CC + L
205	75	25	7	1250	45	CC + L
200	50	50	7	1300	35	L
204	75	25	7	1300	35	L + V
211	90	10	7	1300	35	CC + L + V
203	75	25	7	1350	20	L + V
212	90	10	7	1350	20	CC + L + V
220	90	10	7	1400	10	L + V
214	55.9	44.1	17	1300	20	CC + Wo-I
216	55.9	44.1	17	1325	15	L
215	55.9	44.1	17	1350	10	L
762	30	70	27	1350	120	CC + Wo-II
761	50	50	27	1350	120	CC + Wo-II
774	65	35	27	1350	10	CC + Wo-II
748	80	20	27	1350	10	CC + Wo-II
759	30	70	27	1400	50	Wo-II + L
878	40	60	27	1400	40	L
758	50	50	27	1400	50	L
879	57	43	27	1400	50	CC + L
770	65	35	27	1400	50	CC + L
756	80	20	27	1400	50	CC + L
760	30	70	27	1450	30	L
757	50	50	27	1450	30	L
769	65	35	27	1450	30	CC + L
747	80	20	27	1450	30	CC + L
948	90	10	27	1450	20	CC + L
764	15	85	27	1475	25	Wo-II + L
755	30	70	27	1500	15	L
753	50	50	27	1500	15	L
778	65	35	27	1500	15	L
751	80	20	27	1500	30	CC + L + V
765	90	10	27	1500	15	CC + L + V
775	15	85	27	1515	10	Wo-II + L
766	15	85	27	1550	10	L
775	65	35	27	1550	15	L
749	80	20	27	1550	20	L + V
767	90	10	27	1550	10	L + V
733	100	0	27	1595	5	CC
732	100	0	27	1620	5	L

*Composition of 44.1 wt % $CaSiO_3$ + 55.9 $CaCO_3$ is spurrite + CO_2

ite (Cr) were not encountered in the runs at higher pressures. Figures 2B and 2C show the results for 7 and 27 kbar, respectively, with estimated phase boundaries indicated by dashed lines. A polymorph of $CaSiO_3$ melts congruently between two eutectics. The eutectic liquid between Ca_2SiO_4 and $CaSiO_3$ changes composition only slightly between 1 bar and 7 kbar, but it is enriched in $CaSiO_3$ by 27 kbar. The phase relationships for $CaSiO_3$ (fusion curve and two subsolidus polymorphic transitions) are given in Figure 2D, after Huang and Wyllie (1975a), with the correction of −3 kbar applied (Huang and Wyllie, 1975b). The $CaSiO_3$ transitions have been added to Figures 2B and C. These results provide the univariant curves given in Figure 2D.

Liquids quenched from 7 kbar formed clear glass (#255 and 264) or glass with fibrous quench crystals. Liquids quenched from 27 kbar produced well-formed crystals of wollastonite-II with irregular extinction. Euhedral wollastonite-II prisms crowded with small larnite crystals were produced in subsolidus runs. The distinction between subsolidus and quench wollastonite-II crystals was difficult at temperatures near the solidus (Huang and Wyllie, 1975a), but the quench texture was unambiguous for runs from above the liquidus.

The join $CaCO_3$–$CaSiO_3$ (Table 3, Fig. 3)

The fusion curve for $CaCO_3$ of Irving and Wyllie (1975), corrected by −3 kbar by Huang and Wyllie (1975b), is shown in Figure 3E, and a bracket for 27 kbar is given in Figure 3B.

The phase fields intersected by the join $CaCO_3$–$CaSiO_3$ at 30 kbar were presented by Huang and Wyllie (1974a), and are corrected to 27 kbar in Figure 3B. The corresponding results for 7 kbar are given in Figure 3A. These joins are binary eutectic systems at 7 and 27 kbar, except for the small areas where vapor occurs, indicating that the CO_2-saturated liquids there contained less CO_2 than compositions on the joins. The boundaries of the phase fields including vapor were not precisely located, as indicated by the dashed lines in Figures 3A and B. The binary eutectic reaction between calcite and polymorphs of $CaSiO_3$ is plotted in Figure 3E from the results in Figures 3A and B, and additional runs at 17 kbar (Table 3).

Table 4. Experimental results for the join Ca_2SiO_4–$CaSiO_3$–$CaCO_3$

Run	Starting Composition wt % Ca_2SiO_4	$CaSiO_3$	$CaCO_3$	Press. Kb	Temp. °C	Time min.	Results Assemblages at P and T
268	25	17.5	57.5	7	1150	90	La + Wo-I + CC
271	25	17.5	57.5	7	1175	75	Wo-I + CC + L
269	25	17.5	57.5	7	1200	60	L
270	31.3	13.1	55.6	7	1200	55	La + L
266	25	17.5	57.5	7	1300	30	L
267	37.5	8.8	53.7	7	1300	30	La + L
265	25	17.5	57.5	7	1400	15	L
1031	18	42	40	27	1275	90	La + Wo-I + CC
1032	18	42	40	27	1300	60	La + Wo-I + CC
1030	18	42	40	27	1325	60	L
1049	10	30	60	27	1350	30	CC + L
883	15.5	46.5	38	27	1350	40	Wo-II + L
885	12.5	37.5	50	27	1375	40	Wo-II + L
884	12.5	37.5	50	27	1400	40	L
882	15.5	46.5	38	27	1400	40	L
881	15.5	46.5	38	27	1500	15	L
870	25	25	50	27	1500	20	La + L
875	12.5	37.5	50	27	1550	15	L
886	28	42	30	27	1550	15	La + L
871	25	25	50	27	1650	10	La + L
887	28	42	30	27	1665	10	La + L
888	28	42	30	27	1700	15	L
873	25	25	50	27	1700	10	L
872	25	25	50	27	1750	5	L

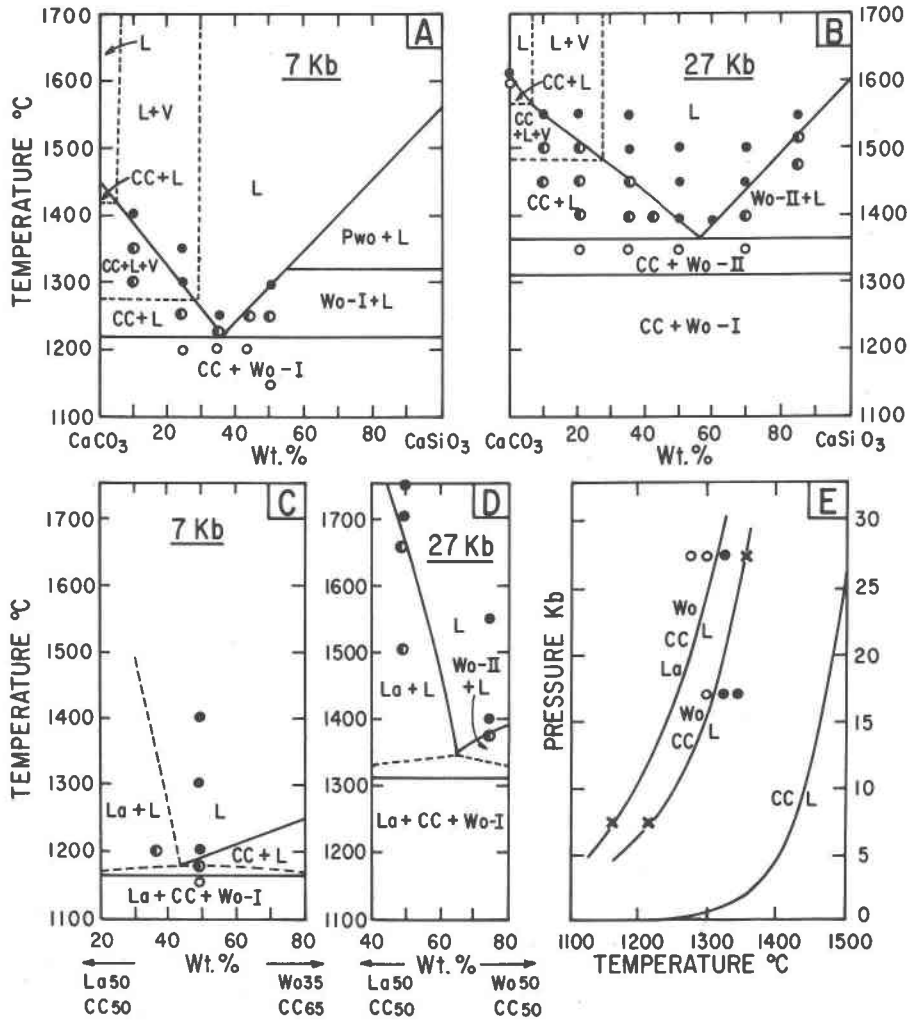

Fig. 3. Experimental results for parts of $CaO–SiO_2–CO_2$. See Fig. 1 for location of the composition joins (3C is part of ab, 3D is part of ac).

Reactions in the triangle $CaCO_3$-$CaSiO_3$-Ca_2SiO_4 (Table 4, Fig. 3)

The joins ab and ac in Figure 1 were selected to locate the positions of ternary field boundaries, and to determine the ternary melting reaction involving calcite, wollastonite, and larnite. Additional mixtures were made within this triangle near the join larnite–CO_2 to provide constraints for the positions of field boundaries.

The ternary eutectic reaction in Figure 3E was located by the runs plotted in Figure 3C, and by runs 1031, 1032, and 1030 of Table 4, plotted in Figure 3E. The liquidus temperatures at points b and c (Fig. 1) for the join $CaCO_3$–$CaSiO_3$ are known (Figs. 3A and 3B), and these values, together with the runs bracketing the liquidus curves in Figures 3C and 3D, place limits on the positions of the piercing points for ternary field boundaries between the fields for the primary crystallization of calcite, larnite, and wollastonite polymorphs, as shown in Figures 3C and 3D. The ternary phase fields intersected above the solidus and below the dashed lines are not depicted.

The join $CaCO_3$-SiO_2 (Table 5, Fig. 4)

The two mixtures made for this join are situated on the crossing joins Ca_2SiO_4–CO_2 and $CaSiO_3$–CO_2 at points d and e, respectively, in Figure 1. The fusion curves for $CaCO_3$ and SiO_2 are known (Fig. 3E; Jackson, 1976, respectively), and these were used in the construction of Figures 4B and C, which show selected runs for the mixtures d and e. These runs determine the position of one univariant decarbonation

Table 5. Experimental results for the join $CaCO_3$–SiO_2

Run*	Starting Composition wt % $CaCO_3$	SiO_2	Press. Kb	Temp. °C	Time	Results Observed products
1018	62.5	37.5	12	1375	60 min	Wo-I + Pwo(tr) + V
1019	62.5	37.5	12	1400	60 min	L
1017	62.5	37.5	12	1475	30 min	L
1046R	62.5	37.5	17	1320	3.5 hr	
	62.5	37.5	17	1250	20 hr	Wo-I + Qz + CC(tr) + L + V
1038	62.5	37.5	17	1275	5 hr	CC + Qz
1045R	62.5	37.5	17	1325	3.5 hr	
	62.5	37.5	17	1275	10 hr	Wo-I + Qz + CC(tr) + L + V
1039	62.5	37.5	17	1300	4 hr	CC + Wo-I + Qz + V
1044	76.9	23.1	17	1300	3 hr	CC + Wo-I + Qz + V
1020	62.5	37.5	17	1325	3.5 hr	Wo-I + Qz + L(tr) + V
1043	76.9	23.1	17	1325	2 hr	CC + Wo-I + L + V
1048	62.5	37.5	17	1350	3.5 hr	Wo-I + Qz + L + V
1050R	62.5	37.5	17	1375	1 hr	
	62.5	37.5	17	1350	3.5 hr	Wo-I + Qz + L(tr) + V
1047	76.9	23.1	17	1350	2 hr	CC + L + V
1021	62.5	37.5	17	1375	50 min	Qz + L + V
1034	76.9	23.1	27	1400	40 min	CC + Qz
1035	76.9	23.1	27	1425	40 min	CC + Qz
1033	62.5	37.5	27	1450	30 min	Qz + L + V
1036	76.9	23.1	27	1450	30 min	CC + Qz + L + V
1052	76.9	23.1	27	1462	30 min	CC + L + V
1051	76.9	23.1	27	1475	30 min	L + V

*R = Reversal Runs

reaction and two melting reactions at 17 kbar, and of a third univariant melting reaction at 27 kbar, and they place in addition geometrical limits on the positions of the liquid compositions in each reaction. The four reactions, meeting at I_2, are given in Figure 4A, together with the definitive runs at 12, 17, and 27 kbar. The reactions are connected with related data as described below.

According to Figure 4, the assemblage CC + Qz dissociates at pressures up to invariant point I_2, and melts incongruently at higher pressures. The dissociation reaction is well defined at 17 kbar by runs at 1300°C for both mixtures (1039 and 1044), which contain all four phases of the reaction. The melting reaction is well defined at 27 kbar by runs 1035, 1036, and 1052 for mixture d, with close confirmation by run 1033 for mixture e.

At 12 and 17 kbar, the assemblage CC + Qz dissociates to Wo + V, and this assemblage melts according to the reactions shown in Figures 4A and 4B. At 12 kbar, the assemblage Wo + V melts directly to liquid (Table 5), but at 17 kbar it melts incongruently to Qz + L. These results require the presence of the singular point, S_1, and the arrangement of melting curves extending down to 1 bar as shown in Figure 4A. The constraints imposed by these runs and the results for Wo and Wo + Qz at 1 bar (Fig. 2A) define the melting curves for Wo and Wo + Qz in the presence of CO_2 rather closely. The intersection of the melting curve for Wo + V with the CC + Qz dissociation reaction generates the invariant point, I_2, which in turn requires the occurrence of the other three curves shown in Figure 4A.

The ternary eutectic for CC + Wo + V is well defined at 17 kbar by runs 1044, 1043, and 1047 for mixture d in Figure 4B, and this is extended down in pressure, approximately parallel with and barely distinguishable from the binary melting curve for CC + Wo (Fig. 3E). It terminates at an invariant point I_1, where it meets the univariant curve for the generation of spurrite (extrapolated from results of Tuttle and Harker, 1957). The position of the ternary eutectic for the melting of CC + Wo + Qz in Figure 4A is estimated, and placed a few degrees below the binary CC + Wo melting curve determined in Figure 3E.

Considering all of the results in Figures 2, 3, and 4, the location of the invariant point I_2 at the intersection of five univariant curves is closely constrained. It is plotted at 18.5 kbar and 1,325°C (believed to be within the limits cited for individual runs).

The results listed in Table 5 for the dissociation of CC + Qz for mixture e, with bulk composition such that the reaction should go completely to Wo + CO_2, show that the actual products were somewhat more complicated. The reaction was signalled clearly at 17 kbar (Fig. 4B) by the appearance of some Wo + Qz in run 1039 at 1,300°C, and the disappearance of calcite in run 1020 at 1,325°C indicates that this was above the reaction temperature—but that charge consisted of very large blades of wollastonite, together with some quartz and a trace of brown quench liquid. We attribute the liquid to reaction between CC + Wo + CO_2 while the reaction was in progress (compare Figs. 4A and B). The liquid became separated from unreacted quartz by the rapid growth of large wollastonite crystals, and the persistence of metastable liquid thus changes the bulk composition of the crystals into the field for Wo-I + Qz + V in Figure 4B.

Two reversal runs were made for the dissociation boundary at 17 kbar. Run 1045R was first held at 1,325°C long enough to reproduce the product of run 1020, large blades of wollastonite together with some quartz and liquid, plus vapor, and then its temperature was lowered to 1,275°C for 10 hours, where the equilibrium assemblage is CC + Qz (run 1038, Fig. 4B). The product included large and small prisms of wollastonite, with abundant quartz and not very much calcite. Another reversal run (R1046R) down

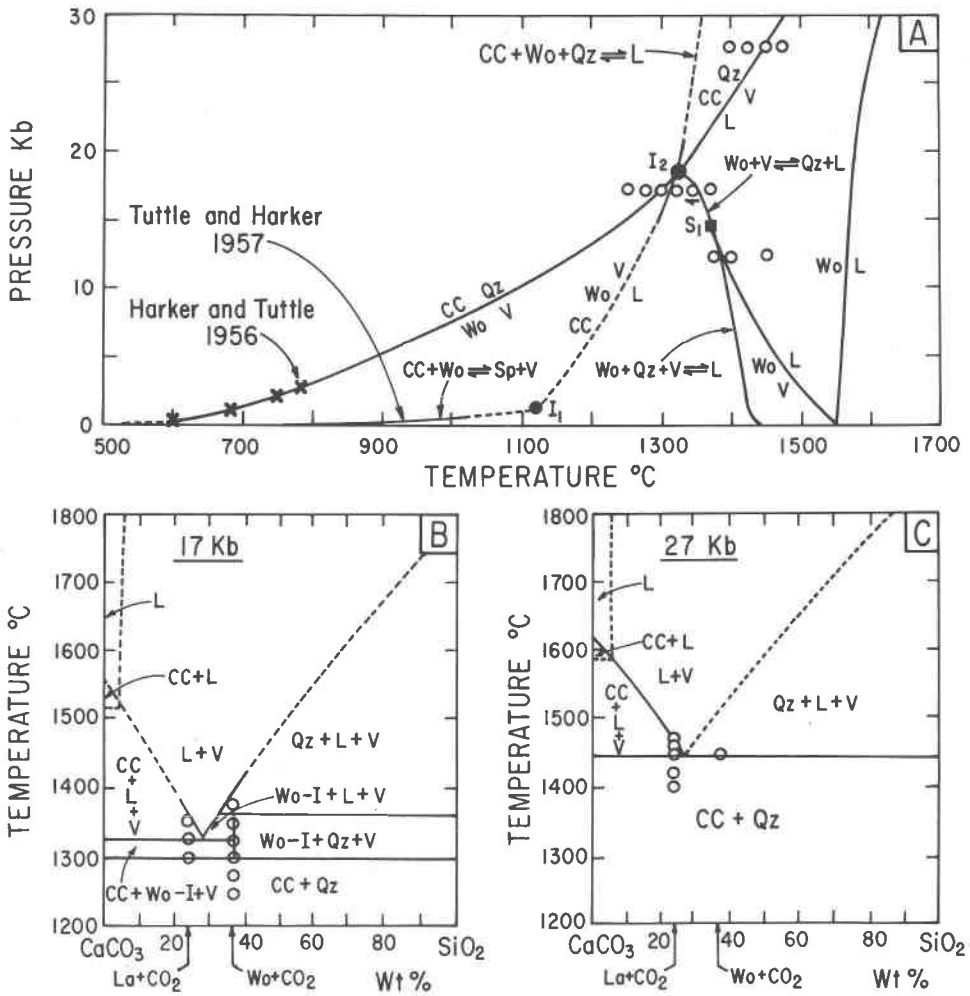

Fig. 4. Reactions between calcite and quartz in $CaO–SiO_2–CO_2$, using compositions d and e from Figure 1. The wollastonite fusion curve is from Huang and Wyllie (1975a), corrected by −3 kbar by Huang and Wyllie (1975b). See text for discussion of recent results of Haselton *et al.* (1978) for calcite–quartz dissociation at 10, 15, and 19 kbar.

to 1,250°C produced similar results. Although reversal is indicated by the reappearance of calcite, and the increase in amount of quartz, it appears that the large crystals of wollastonite, fluxed by the presence of liquid, resist reversal to CC + Qz in the presence of so little CO_2.

Since our diagrams were drafted (in 1975), Haselton *et al.* (1978) have published a curve for this dissociation reaction, based on runs at 10, 15, and 19 kbar. They commented on the rapidity of decarbonation reactions, and were confident that their experiments involving reaction of calcite + quartz mixtures bracketed the equilibria. We drew the reaction in Figure 4A to pass through our results at 17 kbar and the low-pressure determinations of Harker and Tuttle (1956). The 19 kbar result of Haselton *et al.* (1978) at about 1,320°C is coincident with the invariant point I_2 (18.5 kbar–1,325°C), within our respective errors in pressure and temperature measurement; their temperatures of about 1,185° and 1,005°C for 15 and 10 kbar are situated 2–2.5 kbar above the interpolated curve in Figure 4A, and their linear reaction curve extrapolated to low pressures is also about 1 kbar above the high-pressure end of the curve of Harker and Tuttle (1956).

The incongruent melting of Wo + V at 17 kbar was reversed, as shown by run 1050R. The mixture e was first held at 1,375°C for 1 hour, long enough to convert it to Qz + L + V as shown in Figure 4B (run 1021), and then lowered to 1,350°C, where it should react completely to Wo + V, if the mixture was precisely on composition and if equilibrium was

Table 6. Experimental results for the natural spurrite

Run	Press. Kb	Temp. °C	Time hours	Results Run Products
223	5*	1050	4½	La + CC + Sp
224	5*	1050	20 3/4	La + CC + Sp
209	7	1100	2	La + CC
207	7	1100	17	La + CC
742	27	1300	18	La + CC

*Nominal pressure

achieved. The run product consisted of large blades of wollastonite, confirming the reversal, together with some unreacted quench liquid and rounded quartz crystals. There was no calcite.

The join $CaCO_3$-Ca_2SiO_4 and spurrite reactions

A few reconnaissance runs with three mixtures plotted in Figure 1 (not tabulated) showed that at 27 kbar the piercing point for the field boundary between primary larnite and calcite was located between 80% and 85% of $CaCO_3$.

According to the results of Tuttle and Harker (1957), spurrite is produced from CC + Wo at low pressures and high temperatures (Fig. 4A). Boettcher and Wyllie (1969) found melting reactions involving spurrite, dellaite, and calcite at pressures to 10 kbar in the system CaO–SiO_2–CO_2–H_2O. These reactions were at low temperatures in the presence of H_2O-rich vapor. We found no evidence for the persistence of spurrite above the solidus in CaO–SiO_2–CO_2 at pressures greater than 5 kbar. A few runs conducted with a natural spurrite (Table 6) confirmed that spurrite alone was unstable at all pressures above 5 kbar. No spurrite appeared in runs 214–216 in Table 3, for a mixture with composition on the join spurrite–CO_2.

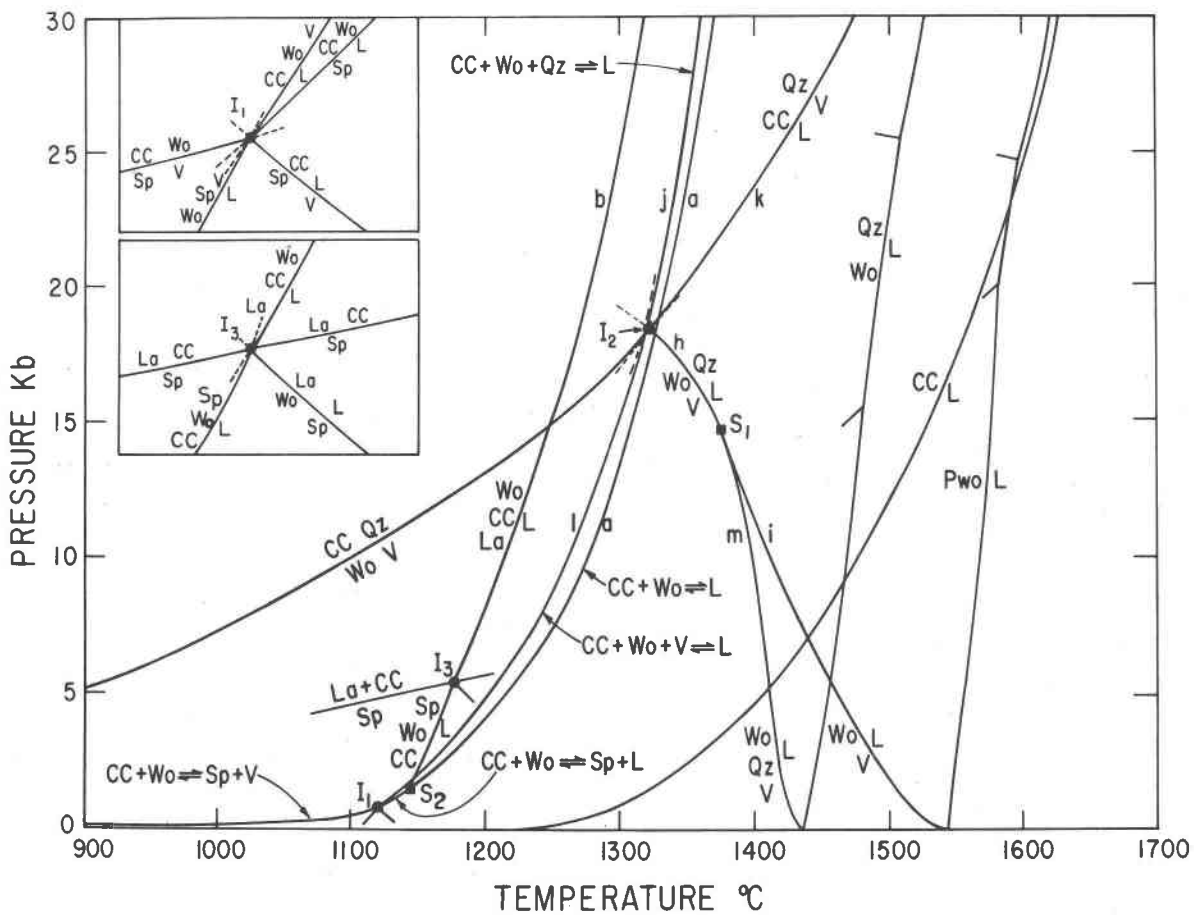

Fig. 5. *PT* projection for the system CaO–SiO_2–CO_2 incorporating experimental data from Fig. 2D, 3E, and 4A together with other constraints discussed in the text. The fusion curve for La + Wo (Fig. 2D), the calcite–aragonite transition (Irving and Wyllie, 1975), and the low-pressure occurrence of Ra (Fig. 2A) have been omitted for graphical clarity. The insets illustrate the reactions around the invariant points I_1 (Fig. 4A) and I_3. The lower-case letters, a, b, j, *etc.* refer to the compositions of liquids in the univariant reactions, as given in the isobaric liquidus diagrams in Fig. 6 and 7.

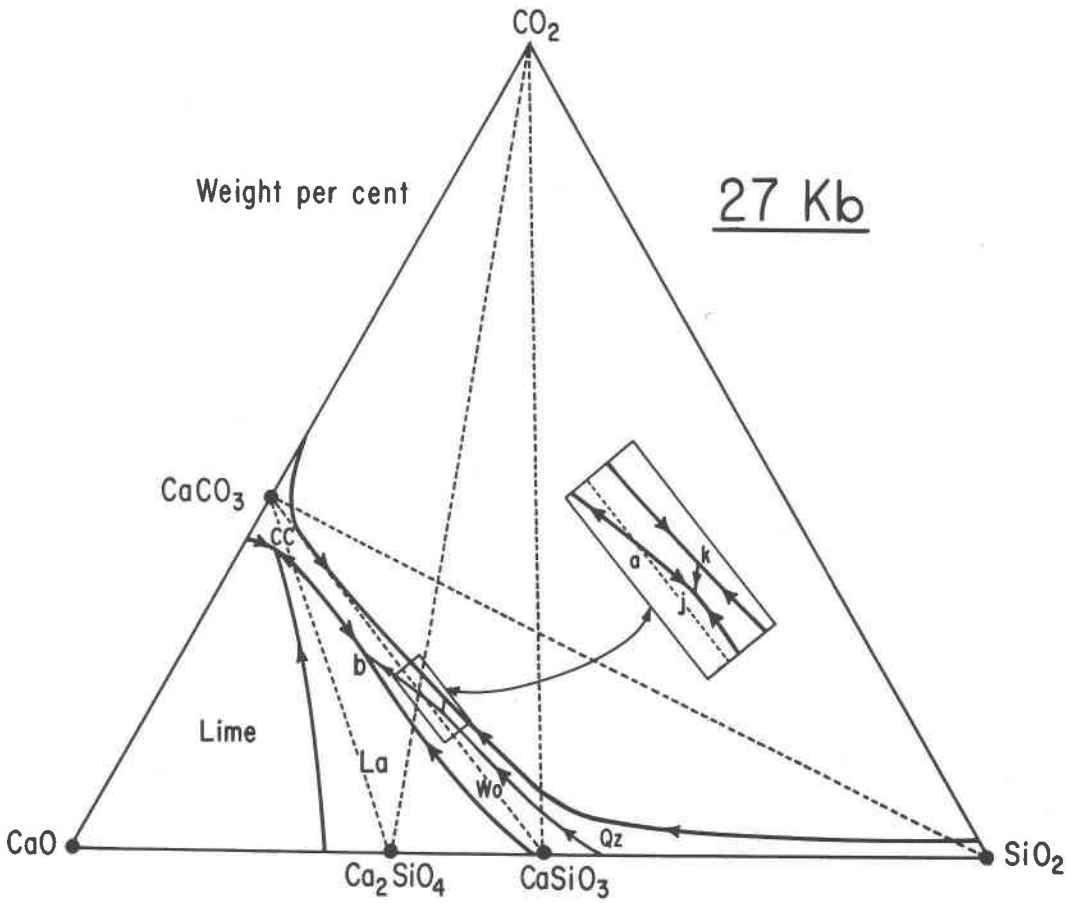

Fig. 6. Liquidus diagram for the system $CaO–SiO_2–CO_2$ at 27 kbar, based on experimental results in Figs. 2, 3, and 4 and additional runs in Table 4. The labeled peritectics and eutectics give liquid compositions for the corresponding univariant reactions in Fig. 5, which give the temperatures for most points in Fig. 6. The temperature maximum on the liquidus surface for Ca_2SiO_4 (Fig. 2C) is suppressed by solution of CO_2, as shown by the La–Wo field boundary.

Phase relations in the system $CaO–SiO_2–CO_2$

Combination of the results plotted in Figures 2D, 3E, and 4A, together with constraints on field boundaries provided by Figures 2, 3, 4, and additional runs in Table 4, permit synthesis of the *PT* projection given in Figure 5, the construction of a detailed liquidus phase diagram for 27 kbar (Fig. 6), and more schematic liquidus diagrams for other pressures (Fig. 7).

Pressure–temperature projection

Figure 5 simply combines the results plotted in previous *PT* diagrams (excluding the fusion curve for La + Wo from Fig. 2D), and adds a schematic interpretation of how spurrite becomes involved at low pressures. The invariant point I_1 required by the intersection of two univariant lines depicted in Figure 4A has three other univariant lines associated with it, as indicated in the upper inset of Figure 5. One of these is an incongruent melting reaction producing spurrite. We have confirmed experimentally that spurrite is eliminated from our starting mixtures by 5 kbar, and this is accomplished in Figure 5 by a singular point, S_2, and the generation of another invariant point, I_3, with the array of univariant curves shown in the inset. At I_3 and higher pressures, spurrite is replaced by La + CC. The melting reactions extending to higher pressures from I_1, I_3, and S_2 are those determined in Figure 3E, and estimated in Figure 4a.

Most of the ternary melting reactions in Figure 5 are identified by a lower-case letter, and the compositions of the isobaric invariant liquids associated with each reaction are given at eutectics and peritectics in Figures 6 and 7, labelled by the same lower-case letters.

Isobaric liquidus diagrams

Figure 6 shows field boundaries separating areas on the liquidus surface at 27 kbar for the primary crystallization of lime, larnite, wollastonite, quartz, and calcite. The enlarged inset gives details around the eutectic liquid, j, between calcite, wollastonite, and quartz. The temperatures at most points on the diagram can be read from Figures 5 and 2D.

The fields for calcite and quartz are bounded on one side by the CO_2-saturated liquidus field boundary. The system CaO–CO_2 and the solubility of CO_2 in $CaCO_3$ liquid at this pressure are known (Huang and Wyllie, 1976), and the fields in Figure 3B with vapor show that the boundary just crosses the join $CaCO_3$–$CaSiO_3$ near the $CaCO_3$ end. The position of the boundary from that region to SiO_2–CO_2 was not determined, but it is known that the solubility of CO_2 in similar silicate liquids remains within the range 5–8% between 10 and 30 kbar (Mysen *et al.*, 1976), decreasing with increasing SiO_2/cafemic oxides. The composition of the liquid k must lie on the line through CO_2 and the eutectic represented on Figure 4C. The temperature maximum at a on the join $CaCO_3$–$CaSiO_3$ corresponds to the eutectic in Figure 3B. The field for primary calcite is constrained by the piercing point on the composition join $CaCO_3$–Ca_2SiO_4 between 80 and 85% $CaCO_3$, and the other field boundaries are constrained by runs on mixtures within the composition triangle $CaCO_3$–Ca_2SiO_4–$CaSiO_3$ (Fig. 1), as shown by Figure 3D (see also Fig. 3C), and runs 883 and 886 in Table 4, for example.

According to Figure 6, quartz and calcite melt incongruently at 27 kbar to produce liquid (k) and CO_2; with cooling of the liquid, calcite and quartz are coprecipitated along the field boundary kj, and joined by wollastonite at the eutectic j. At pressures below I_2, as shown in Figure 5, quartz and calcite dissociate at temperatures below the solidus, indicating that the field boundary kj of Figure 6 does not exist below 18.5 kbar. The sequence of changes for primary phase fields on the liquidus surface as a function of increasing pressure and carbonation is shown in Figure 7.

Wyllie and Haas (1965, Fig. 5) presented a schematic liquidus diagram for CaO–SiO_2–CO_2 at 1 kbar, which was similar to that for 5 kbar in Figure 7A, except for the inclusion of a large field for the crystallization of spurrite. According to Figure 5, spurrite is not stable on the liquidus at pressures above 5 kbar, and Figure 7A represents the phase relationships in the interval 5–15 kbar. Note that the fields for calcite and quartz are widely separated, and the field for calcite is smaller than at 27 kbar, as determined by the position of the eutectic a, between $CaCO_3$ and $CaSiO_3$ (compare Figs. 3A and 3B).

At the singular point S_1 near 15 kbar (Fig. 5), the expanding field for quartz just reaches the join $CaSiO_3$–CO_2 (Fig. 7B), and at higher pressures Wo + CO_2 no longer melts congruently but melts incongruently to Qz + L (Fig. 5). This is represented in Figure 7C by extension of the quartz field across the Wo–CO_2 join to point h, which replaced points m and i in Figure 7A (compare lines m, i, and h in Fig. 5). The compositions of liquids l and h in Figure 7C for 17 kbar are determined by projections from the peritectic and eutectic represented in Figure 4B.

With increasing pressure through Figures 7A, B, and C, the fields for calcite and quartz enlarge, coming closer together at the expense of wollastonite; at the invariant point I_2, 18.5 kbar, the fields for calcite and quartz just meet, as shown in Figure 7D. The assemblage CC + Qz which dissociated to Wo + CO_2 at lower pressures is joined at 18.5 kbar by the invariant liquid, I_2 in Figure 7D. At higher pressures, the field for wollastonite does not reach the CO_2-saturated liquidus, and the liquids l and h of Figure 7C are replaced by k and j of Figure 6. The assemblage CC + Qz then dissociates with melting to L + CO_2 (follow curves l, h, k, and j in Fig. 5).

These changes are a consequence of the carbonation of silicates with increasing pressure. Up to 18.5 kbar, wollastonite is stable with CO_2, and there is a solidus curve, i–h in Figure 5, showing the effect of CO_2 on the fusion of wollastonite. At I_2, a pressure is reached where Wo + CO_2 is carbonated to produce CC + Qz, and at higher pressures any CO_2 present with wollastonite is converted to calcite with formation of quartz, and the silicate assemblage then melts with calcite (reaction j in Fig. 5) and not with free CO_2. Only if there is enough CO_2 to carbonate the wollastonite completely can melting occur with vapor, and this is shown by the fusion curve k in Figure 5.

The inset in Figure 5 shows that reactions for the melting and carbonation of the assemblage spurrite + CO_2 which meet at invariant point I_1 are associated with an array of additional melting reactions equivalent to those around invariant point I_2.

Comparison with other systems

The general arrangement of reaction curves described and illustrated for the system CaO–SiO_2–CO_2

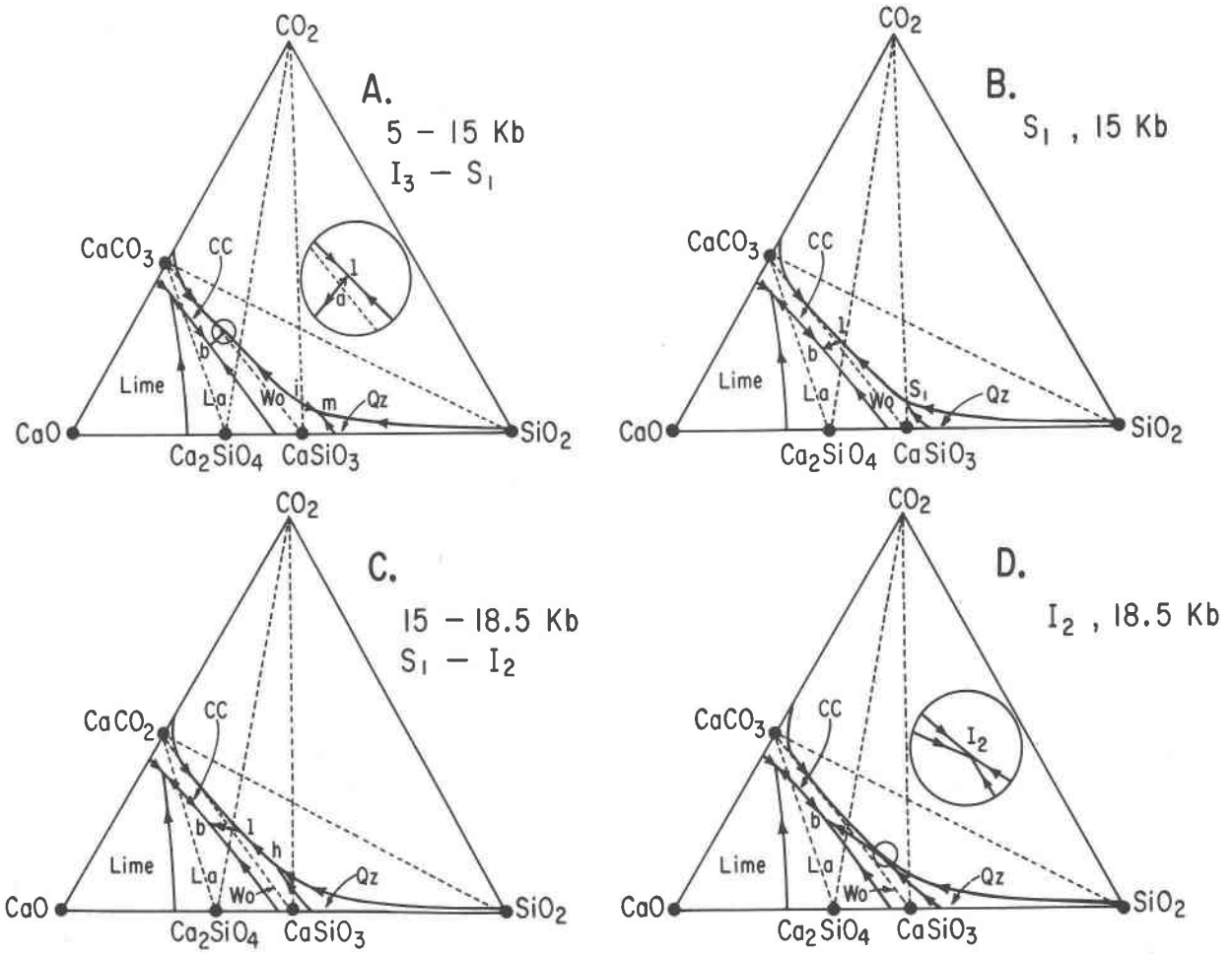

Fig. 7. Isobaric liquidus diagrams for the system $CaO–SiO_2–CO_2$ showing the effect of pressure on the compositions of eutectic and peritectic liquids, and the associated changes in arrangements of areas of primary crystallization of minerals, for pressure intervals identified in Fig. 5. Critical changes occur at S_1 (B) and at I_2 (D); see Fig. 6 for higher pressures. See text for discussion of conditions below I_3 and I_1 (Fig. 5).

is common to other silicate–volatile component systems in which the volatile component forms a compound at high pressures with the silicate components. With CO_2 carbonation reactions produce carbonates, and with H_2O hydration reactions produce hydrous minerals. The dissociation reactions intersect the silicate–volatile component solidus curves at invariant points, introducing the compound into the solidus assemblages at pressures higher than the invariant points.

The phase relationships around invariant point I_2 in Figure 5 are directly analogous to those deduced by Wyllie and Huang (1976b) for the system $MgO–SiO_2–CO_2$. The phase relationships differ in the latter system because there is no magnesian equivalent of spurrite, and there are three invariant points corresponding to three successive carbonation reactions involving univariant combinations of forsterite, enstatite, quartz, magnesite, and CO_2. The carbonate is stable to higher temperatures in the calcium system than in the magnesium system, which means that a higher pressure is required to produce the same degree of carbonation in the magnesium system, and the invariant points for equivalent carbonation reactions at the solidus for the magnesium system therefore occur at higher pressures. This is confirmed by the following comparisons.

Invariant points involving carbonate, oxide, liquid, and CO_2 occur at 40 bars in $CaO–CO_2$ (Baker, 1962), and at 23 kbar in $MgO–CO_2$ (Irving and Wyllie, 1975; Huang and Wyllie, 1976). Invariant point I_2 in the system $CaO–SiO_2–CO_2$ occurs at 18.5 kbar (Fig. 5), whereas the corresponding invariant point in the system $MgO–SiO_2–CO_2$ involving $MgCO_3$, $MgSiO_3$,

SiO_2, liquid, and CO_2 occurs near 58 kbar (estimated by Wyllie and Huang, 1976b).

The greater stability of carbonate in calcium compared with magnesium systems is also indicated by the size of the liquidus surfaces for primary crystallization of carbonate. Huang and Wyllie (1974a) determined the phase fields intersected by the joins $MgCO_3$–$MgSiO_3$ and $CaCO_3$–$CaSiO_3$ at 30 kbar (later corrected to 27 kbar, Huang and Wyllie, 1975b). The content of dissolved silicate component at the edges of the carbonate fields is about 9% for $MgCO_3$ and almost 60% for $CaCO_3$ (see Fig. 3B).

Figures 6 and 7 show that the size of the liquidus surface for calcite increases with increasing pressure, with the content of dissolved silicate on the CC–Wo join increasing from about 35% at 7 kbar to about 60% at 27 kbar (Figs. 3A and 3B). According to Figures 6 and 7, it appears that most of the expansion of the calcite field is accomplished by the pressure of I_2, where the melting silicate assemblages are fully carbonated to wollastonite plus quartz. Similar relationships may be anticipated in the system MgO–SiO_2–CO_2. The very small field for primary magnesite at 27 kbar is probably represented in the system CaO–SiO_2–CO_2 by a small field for primary calcite at a much lower pressure, probably below I_1 in Figure 5, as estimated by Wyllie and Haas (1965, Fig. 5). The magnesite field should expand with increasing pressure (confirmed by R. Wendlandt, personal communication, 1979). It could even approach the central part of the join $MgCO_3$–$MgSiO_3$ at a pressure near 58 kbar, where the magnesite and quartz fields meet at the CO_2-saturated liquidus boundary, directly analogous to the point I_2 in Figure 7D. This would entail an expansion of the primary $MgCO_3$ field from about 10% silicate to about 50% silicate in the pressure interval from about 30 to 60 kbar, with significant petrological implications; this merits experimental study.

In the system CaO–MgO–SiO_2–CO_2 the additional minerals diopside and dolomite, and solid-solution relationships among the pyroxenes and the carbonates, introduce many more dissociation/carbonation reactions. Despite the added complexity, the pattern of phase relationships remains the same. Each of the carbonation reactions reaches the solidus for melting of the silicate–CO_2 assemblage, and introduces a carbonated mineral into the solidus assemblage at higher pressures (Wyllie and Huang, 1975, 1976a; Eggler, 1976).

The phase relationships in the system MgO–SiO_2–H_2O, as analyzed by Ellis and Wyllie (1979), are similarly analogous to those in the systems MgO–SiO_2–CO_2 and CaO–SiO_2–CO_2. In the system MgO–SiO_2–H_2O, the invariant point involving $MgSiO_3$, Mg_2SiO_4, $Mg(OH)_2$, and H_2O vapor is estimated to occur at a pressure of near 90 kbar. This is much higher than the pressure near 43 kbar for the corresponding invariant point in the system MgO–SiO_2–CO_2.

Petrological applications

Metamorphism

The system CaO–SiO_2–CO_2 contains mineral assemblages corresponding to siliceous limestones or marbles. The familiar low-pressure metamorphic reactions in Figure 5 merit no additional attention. The low-pressure melting reactions may have relevance to some skarns, especially in the presence of additional volatile components, but we have no new data in this area.

Subduction

If limestones or calcite veins in oceanic basalts are subducted with oceanic lithosphere, they will be subjected to metamorphism at very high pressures, and they may become involved in melting processes at great depths. There are divergent opinions about the extent to which oceanic sediments are subducted, or scraped off and accreted laterally at continental margins or island arcs.

Mass balance calculations for trace elements and lead isotope compositions for andesites and oceanic sediments led Armstrong (1971) to conclude that, on the average, sediment contamination is required to explain the chemistry of magmas generated in subduction zones (but not necessarily in every subduction zone). Magaritz and Taylor (1976) concluded from their stable isotope studies of the Franciscan formation, andesites, and batholiths that a major component of the carbon and hydrogen derived from the mantle conceivably could represent recycled material from subducted sediments.

There is convincing evidence that calcareous material constitutes an integral part of the basaltic ocean crust, indicating that some calcite is subducted. Results from deep drilling on Leg 37 of the Deep Sea Drilling Project, for example, included abundant unconsolidated and lithified foram-bearing nannofossil ooze within the basalt sequence of ocean crust layer 2 (*Geotimes*, 1974). Some recrystallized ooze persists as veins and irregular zones in basalt to a depth of at least 544 m.

There is also good reason to suppose that, even if

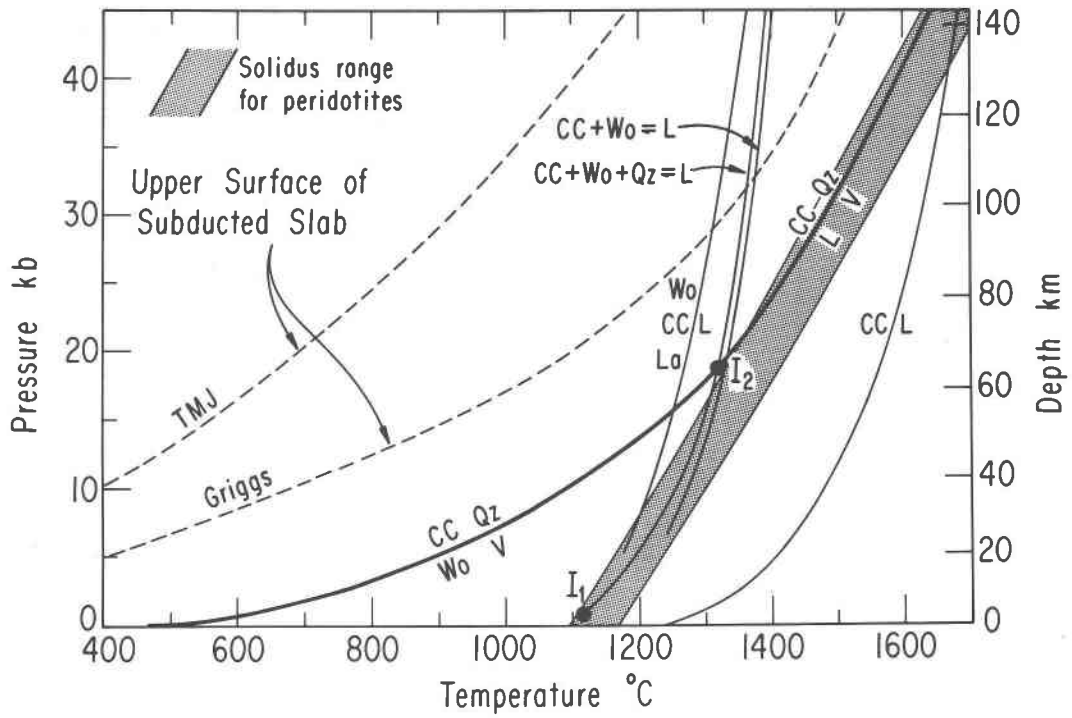

Fig. 8. Reactions involving calcite–quartz assemblages, selected from Fig. 7, compared with approximate range of reported solidus curves for peridotite (Irving and Wyllie, 1973). The dashed lines give two estimates for the temperature along the surface of subducted oceanic lithosphere (Griggs, 1972; Toksöz *et al.*, 1971, TMJ). The calcite–aragonite transition (Irving and Wyllie, 1975) is situated between these two dashed curves.

most sediments are accreted laterally, some of them are subducted. Moore (1975) pointed out that the biogenic oozes that initially cover young oceanic crust, calcareous ooze followed by siliceous ooze, become lithified during transportation to convergent plate boundaries. He suggested that these tough rocks, with densities similar to that of the underlying basalt, might be subducted, whereas the overlying pelagic–terrigenous muds and ocean-trench clastic units were more likely to be deformed and accreted.

Figure 8 reproduces from Figure 5 the reactions that could affect subducted limestones or siliceous limestones, and compares these with two estimates of the temperature along the surface of a subducted slab, and the pressure–temperature range reported for solidus curves of peridotite (Irving and Wyllie, 1973). The melting temperatures of siliceous limestones correspond closely with temperatures of beginning of melting of mantle peridotite. The fusion curve for calcite or limestone is situated at considerably higher temperatures, although the difference decreases at the higher pressures.

Addition of the calcite–aragonite transition (Irving and Wyllie, 1973, 1975) to Figure 8 would indicate that for the thermal model of Griggs (1972), calcite becomes converted to aragonite at a depth greater than 140 km. For cooler models, however, the transition occurs at shallower depths, and the whole length of the TMJ temperature curve plotted in Figure 8 is situated within the aragonite field.

The dissociation curves and fusion curves for siliceous limestone and pure limestone remain well above estimated temperatures for subducted ocean crust, suggesting that these sediments could be carried to considerable depth without change, other than recrystallization to marble and transformation to aragonite.

Although the thermal models for subduction zones do not include temperatures high enough to cross the subsolidus wollastonite-producing reaction in Figure 8, the effect of H_2O released by dehydration of the hydrated ocean crust (see Wyllie, 1973, 1979, for review) would be to lower the dissociation temperature across a divariant surface for the reaction occurring in the presence of H_2O–CO_2 vapors, as illustrated by the dash–dot lines in Figure 9. The availability of H_2O would affect all reactions in Figure 8, but evaluation of the detailed effect of H_2O on reactions occurring in a subducted slab including limestone is not warranted here. There are large uncertainties about

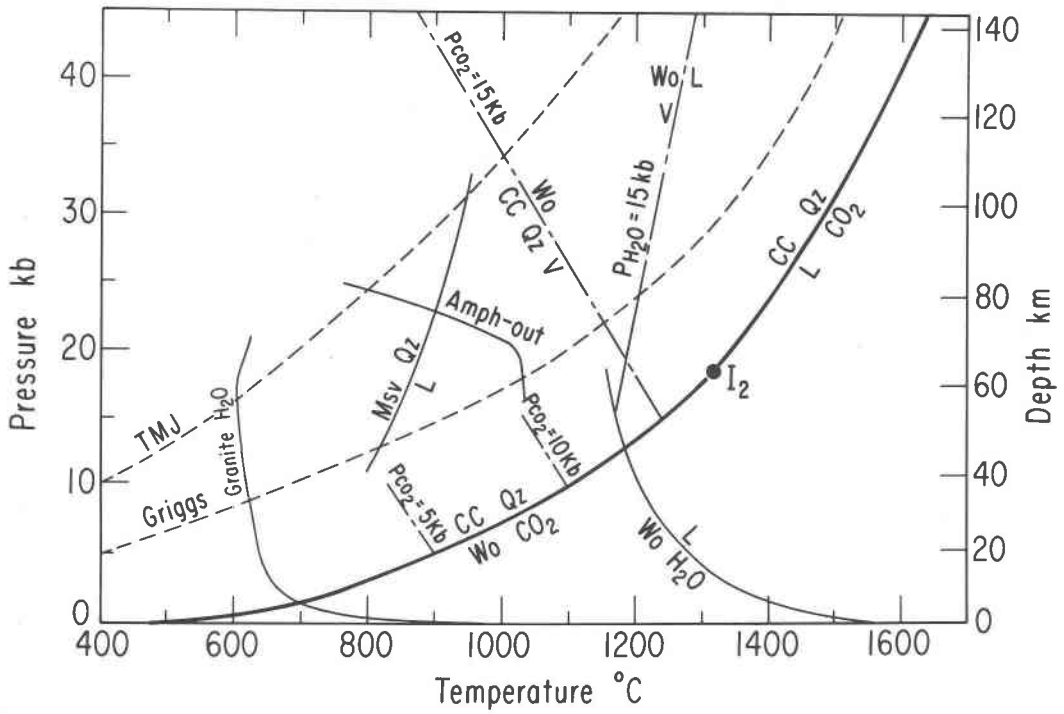

Fig. 9. Temperature curves (dashed) and calcite–quartz reactions from Fig. 8. Other reactions are: solidus for granite–H_2O (Boettcher and Wyllie, 1968), for muscovite(Msv)–quartz (Huang and Wyllie, 1974b), and for wollastonite–H_2O (Huckenholz and Yoder, 1974); amphibole breakdown in gabbro–H_2O (Lambert and Wyllie, 1972). The dash–dot lines representing decarbonation in the presence of CO_2–H_2O mixtures for conditions of constant P_{eCO_2} were calculated from equation 2 of Greenwood (1967), using entropy of CO_2 at 1 kbar and 680°C from Sharp (1962), and other data from Robie and Waldbaum (1968). These contours illustrate the shape of the divariant dissociation surface, and precise values are not significant for present purposes. The estimated position of the constant P_{eH_2O} contour for the divariant fusion surface for wollastonite in the presence of H_2O–CO_2 mixtures illustrates the different geometrical shape of the solidus surfaces.

the temperature distribution in subducted slabs and the dependent distribution and migration of H_2O. The situation becomes complicated by hydrous melting of the gabbroic crust.

Figure 9 illustrates the possible effect of H_2O on specific reactions, considering each independently of the others, and neglecting the fact that these reactions overlap in P–T–CO_2–H_2O space. The calcite–quartz reactions and the two estimated slab-surface temperatures are reproduced from Figure 8. The curves for granite–H_2O and muscovite–quartz show the effect of H_2O on magma generation within any micaceous sediments that might be subducted (Huang and Wyllie, 1973). The amphibole-out curve shows a limit for the release of H_2O from the main gabbroic part of the crust, either for escape into the overlying subducted sediments and mantle or for direct participation in the melting of amphibolite (for review see Wyllie, 1979).

Partial dissociation of subducted limestones caused by migrating H_2O would begin with the formation of wollastonite, as shown in Figure 9 by the calculated contours for constant P_{eCO_2}, which map the divariant surface for the calcite–quartz–vapor dissociation. If this rock escaped involvement with silicate magmas, then one of the temperature estimates does cross the melting curves for assemblages involving wollastonite with calcite and quartz. If melting occurs, Figures 6 and 7 show that the liquids produced would have carbonatitic compositions, consisting of approximately 50% $CaCO_3$ and 50% $CaSiO_3$.

If dehydration of the subducted slab should introduce H_2O into limestone undergoing partial fusion, the melting reactions become represented by divariant surfaces with shapes different from the dissociation reaction, as indicated by the single contour for the wollastonite–vapor reaction in Figure 9. Addition of H_2O would lower the temperatures of melting reactions for vapor-absent limestones and for limestones with CO_2. At depths where partial fusion of metamorphosed siliceous limestones could begin, there is little H_2O left in the subducted slab to enhance melting.

There is a good prospect that marbles produced

from the lithified pelagic limestones would permit only limited access to migrating H_2O, and that the reacting limestones would force the diffusing fluid compositions towards CO_2 enrichment, which would reduce the extent of wollastonite production at temperatures existing within the slab (Fig. 9). Therefore much of the subducted calcite would probably escape dissociation and melting and be carried down to considerable depths (Figs. 8 and 9), possibly for long-term storage of carbon in the mantle either as aragonite, or as diamond if the carbonate is reduced in whole or in part. Aragonite masses should react marginally with mantle peridotite to produce dolomite or magnesite, depending on depth (Wyllie, 1977; Eggler, 1978).

The upper mantle

The system $CaO–SiO_2–CO_2$ forms one side of the tetrahedron for the system $CaO–MgO–SiO_2–CO_2$, which has been used as a model for the effect of CO_2 on the mineralogy of, and magma generation in, the upper mantle (*e.g.* Eggler, 1974, 1978; Wyllie and Huang, 1975, 1976b). Wyllie and Huang (1976b, Figs. 2 and 8) used results from Figures 4A and 6 as limits for their construction of partly schematic phase relationships in the quaternary system for (1) the sequence of decarbonation (or carbonation) reactions, and (2) the CO_2-saturated liquidus field relationships. The general pattern of phase relationships described around the invariant point I_2 (Figs. 4A and 5) is repeated in the quaternary system, and this may be applied with confidence to mantle peridotites (Wyllie, 1977, 1978, 1979; Eggler, 1975, 1976, 1978).

Carbonatites

$CaO–SiO_2–CO_2$ is the simplest system with compositions representing silicate and carbonatite magmas. Igneous wollastonite occurs in some carbonatites and in some alkalic rocks associated with carbonatites (Heinrich, 1966, p. 195). Figures 5, 6, and 7 show conditions under which wollastonite and calcite may be coprecipitated from a melt in this simple system. Pressure must be greater than invariant point I_1. Temperatures are somewhat higher than those normally assigned to carbonatite intrusions (Heinrich, 1966, p. 281–286; Tuttle and Gittins, 1966, *e.g.* p. 6, 148), but addition of other components such as H_2O would lower liquidus temperatures (Wyllie and Haas, 1965, 1966; Boettcher and Wyllie, 1969).

Wyllie and Haas (1965, Fig. 5) presented a schematic diagram for $CaO–SiO_2–CO_2$ at 1 kbar, relying heavily on results for $CaO–SiO_2$ at 1 bar (Fig. 2A) and the results of Eitel (1923) for the join $Ca_2SiO_4–CaCO_3$ in the presence of CO_2 at 120 bars. In their diagram, fields for the crystallization of larnite and spurrite were extended to the CO_2-saturated field boundary between the fields for calcite and wollastonite (see Fig. 7A), and the thermal barrier associated with larnite in the system $CaO–SiO_2$ (Fig. 2 shows high liquidus temperature for larnite) was extended to the CO_2–saturated boundary. In fact, this inferred situation can exist only at pressures below invariant point I_1. At higher pressures, as shown by Figure 7A and the inset in Figure 5, the spurrite and larnite fields become separated from the CO_2-saturated field boundary by the growth and meeting of the fields for calcite and wollastonite. In addition, the field for spurrite disappears on the liquidus at pressures above I_3 (Figs. 5 and 7A).

Wyllie and Haas (1965, 1966) noted that the large thermal barrier corresponding to the melting of larnite in the presence of CO_2, or of $CO_2–H_2O$ vapors, separated liquids with compositions corresponding to normal silicate magmas (those with SiO_2/CaO higher than in Ca_2SiO_4) from the lower-temperature synthetic carbonatite magmas capable of precipitating calcite. Figures 5 and 7A show that this high thermal barrier exists only at pressures below I_1. It is eliminated at this pressure by the carbonation reaction for spurrite–CO_2 and by solution of CO_2 in the liquid, which brings the primary fields for wollastonite and calcite together in eutectic fashion around the CO_2-side of the thermal barrier.

The thermal ridge on the liquidus surface of the system $CaO–SiO_2–CO_2–H_2O$, corresponding to the join $Ca_2SiO_4–CO_2–H_2O$ (Wyllie and Haas, 1965, Fig. 14), must retreat across the surface from the CO_2 side at I_1 toward the H_2O side at higher pressures, in a way similar to that described in detail by Ellis and Wyllie (1980) for $MgO–SiO_2–CO_2–H_2O$. The liquidus field for wollastonite then extends across the fields for larnite and spurrite to meet the field for calcite directly (see Fig. 7A) as the thermal barrier is eliminated, instead of in the indirect way proposed by Wyllie and Haas, (1966, Figs. 8 and 10).

Acknowledgments

This research was supported by NSF grant EAR 76-20410 (Earth Sciences Section).

References

Armstrong, R. L. (1971) Isotopic and chemical constraints on models of magma genesis in volcanic arcs. *Earth Planet. Sci. Lett., 12,* 137–142.

Baker, E. H. (1962) The calcium oxide–carbon dioxide system in

the pressure range 1–300 atmospheres. *J. Chem. Soc., 87,* 464–470.

Boettcher, A. L. (1975) Experimental igneous petrology. *Rev. Geophys. Space Phys., 13,* 75–79.

——— and P. J. Wyllie (1968) Melting of granite with excess water to 30 kilobars pressure. *J. Geol., 76,* 235–244.

——— and ——— (1969) The system $CaO–SiO_2–CO_2–H_2O$: III. Second critical end-point on the melting curve. *Geochim. Cosmochim. Acta, 33,* 611–632.

Boyd, F. R., P. M. Bell, J. L. England and M. C. Gilbert (1967) Pressure measurements in single-stage apparatus. *Carnegie Inst. Wash. Year Book, 65,* 410–414.

Delaney, J. R., D. W. Muenow and D. G. Graham (1978) Abundance and distribution of water, carbon and sulfur in the glassy rims of submarine pillow basalts. *Geochim. Cosmochim. Acta, 42,* 581–594.

Eggler, D. H. (1974) Effect of CO_2 on the melting of peridotite. *Carnegie Inst. Wash. Year Book, 73,* 215–224.

——— (1975) Peridotite–carbonate relations in the system $CaO–MgO–SiO_2–CO_2$. *Carnegie Inst. Wash. Year Book, 74,* 468–474.

——— (1976) Does CO_2 cause partial melting in the low-velocity layer of the mantle? *Geology, 4,* 69–72.

——— (1978) The effect of CO_2 upon partial melting of peridotite in the system $Na_2O–CaO–Al_2O_3–MgO–SiO_2–CO_2$ to 35 kb, with an analysis of melting in a peridotite–$H_2O–CO_2$ system *Am. J. Sci., 278,* 305–343.

Eitel, W. (1923) Uber das binare System $CaCO_3–Ca_2SiO_4$ und den Spurrit. *Neues Jahrb. Mineral., Beilage-Band, 48,* 63–74.

Ellis, D. and P. J. Wyllie (1979) Hydration and melting reactions in the system $MgO–SiO_2–H_2O$ at pressures up to 100 kilobars. *Am. Mineral., 64,* 41–48.

——— and ——— (1980) Phase relations and their petrological implications in the system $MgO–SiO_2–H_2O–CO_2$ at pressures up to 100 kbar. *Am. Mineral., 65,* in press.

Geotimes (1974) Deep Sea drilling project, 16–18 (December).

Green, H. W. and S. V. Radcliffe (1975) Fluid precipitates in rocks from the earth's mantle. *Geol. Soc. Am. Bull., 86,* 846–852.

Greenwood, H. J. (1967) Mineral equilibria in the system $MgO–SiO_2–H_2O–CO_2$. In P. H. Abelson, Ed., *Researches in Geochemistry,* Vol. II, p. 542–547. Wiley, New York.

Griggs, D. T. (1972) The sinking lithosphere and the focal mechanism of deep earthquakes. In E. C. Robertson, Ed., *The Nature of the Solid Earth,* p. 361–384. McGraw-Hill, New York.

Harker, R. I. and O. F. Tuttle (1956) Experimental data on the P_{CO_2}–T curve for the reaction: calcite + quartz = wollastonite + carbon dioxide. *Am. J. Sci., 254,* 239–256.

Haselton, H. T., W. E. Sharp and R. C. Newton (1978) CO_2 fugacity at high temperatures and pressures from experimental decarbonation reactions. *Geophys. Res. Lett., 5,* 753–756.

Heinrich, E. W. (1966) *The Geology of Carbonatites.* Rand McNally, Chicago.

Huang, W. L. and P. J. Wyllie (1973) Muscovite dehydration and melting in deep crust and subducted oceanic sediments. *Earth Planet. Sci. Lett., 18,* 133–136.

——— and ——— (1974a) Eutectic between wollastonite II and calcite contrasted with thermal barrier in $MgO–SiO_2–CO_2$ at 30 kilobars, with applications to kimberlite–carbonatite petrogenesis. *Earth Planet. Sci. Lett., 24,* 305–310.

——— and ——— (1974b) Melting relations of muscovite with quartz and sanidine in the system $K_2O–Al_2O_3–SiO_2–H_2O$ to 30 kilobars and an outline of paragonite melting relations. *Am. J. Sci., 274,* 378–395.

——— and ——— (1975a) Melting and subsolidus phase relationships for $CaSiO_3$ to 35 kilobars pressure. *Am. Mineral., 60,* 213–217.

——— and ——— (1975b) Melting reactions in the system $NaAlSi_3O_8–KAlSi_3O_8–SiO_2$ to 35 kilobars, dry and with excess water. *J. Geol., 83,* 737–748.

——— and ——— (1976) Melting relationships in the systems $CaO–CO_2$ and $MgO–CO_2$ to 33 kilobars. *Geochim. Cosmochim. Acta, 40,* 129–132.

Huckenholz, H. G. and H. S. Yoder (1974) The gehlenite–H_2O and wollastonite–H_2O systems. *Carnegie Inst. Wash. Year Book, 73,* 440–443.

Irving, A. J. and P. J. Wyllie (1973) Melting relationships in $CaO–CO_2$ and $MgO–CO_2$ to 36 kilobars, with comments on CO_2 in the mantle. *Earth Planet. Sci. Lett., 20,* 220–225.

——— and ——— (1975) Subsolidus and melting relationships for calcite, magnesite, and the join $CaCO_3–MgCO_3$ to 36 kilobars. *Geochim. Cosmochim. Acta, 39,* 35–53.

Jackson, I. (1976) Melting of the silica isotypes SiO_2 BeF_2 and GeO_2 at elevated pressures. *Phys. Earth Planet. Interiors, 13,* 218–231.

Lambert, I. B. and P. J. Wyllie (1972) Melting of gabbro (quartz eclogite) with excess water to 35 kilobars, with geological applications. *J. Geol., 80,* 693–708.

Magaritz, M. and H. P. Taylor (1976) Oxygen, hydrogen and carbon isotope studies of the Franciscan formation, Coast Ranges, California. *Geochim. Cosmochim. Acta, 40,* 215–234.

Moore, J. C. (1975) Selective subduction. *Geology, 3,* 530–532.

Mysen, B. O., D. H. Eggler, M. G. Seitz and J. R. Holloway (1976) Carbon dioxide in silicate melts and crystals. I. Solubility measurements. *Am. J. Sci., 276,* 455–479.

Robie, R. A. and D. R. Waldbaum (1968) Thermodynamic properties of minerals and related substances at 298.15°K (25.0°C) and one atmosphere (1.0132 bars) pressure and at higher temperatures. *U. S. Geol. Surv. Bull. 1259.*

Sharp, W. E. (1962) The thermodynamic functions for carbon dioxide in the range 40 to 1,000°C and 1 to 1,400 bars. *Univ. Calif. Lawrence Livermore Radiation Labs. Publication Number UCRL-7168.* Livermore, California.

Toksöz, M. N., J. W. Minear and B. R. Julian (1971) Temperature field and geophysical effects of a downgoing slab. *J. Geophys. Res., 76,* 1113–1138.

Tuttle, O. F. and J. Gittins (1966) *Carbonatites.* Interscience, New York.

——— and R. I. Harker (1957) Synthesis of spurrite and the reaction wollastonite + calcite = spurrite + carbon dioxide. *Am. J. Sci., 255,* 226–234.

Wyllie, P. J. (1973) Experimental petrology and global tectonics: a preview. *Tectonophysics, 17,* 189–209.

——— (1977) Mantle fluid compositions buffered by carbonates in peridotite–$CO_2–H_2O$. *J. Geol., 85,* 187–207.

——— (1978) Mantle fluid compositions buffered in peridotite–$CO_2–H_2O$ by carbonates, amphibole, and phlogopite. *J. Geol., 86,* 687–713.

——— (1979) Magmas and volatile components. *Am. Mineral., 64,* 469–500.

——— and J. L. Haas (1965) The system $CaO–SiO_2–CO_2–H_2O$: I. Melting relationships with excess vapor at 1 kilobar pressure. *Geochim. Cosmochim. Acta, 29,* 871–892.

——— and ——— (1966) The system $CaO–SiO_2–CO_2–H_2O$: II. The petrogenetic model. *Geochim. Cosmochim. Acta, 30,* 525–544.

——— and W. L. Huang (1975) Influence of mantle CO_2 in the generation of carbonatites and kimberlites. *Nature, 257,* 297–299.

——— and ——— (1976a) Carbonation and melting reactions in the system $CaO–MgO–SiO_2–CO_2$ at mantle pressures with geophysical and petrological applications. *Contrib. Mineral. Petrol., 54,* 79–107.

——— and ——— (1976b) High CO_2 solubilities in mantle magmas. *Geology, 4,* 21–24.

——— and O. F. Tuttle (1960) The system $CaO–CO_2–H_2O$ and the origin of carbonatites. *J. Petrol., 1,* 1–46.

Manuscript received, May 7, 1979;
accepted for publication, October 3, 1979.